Atmos. Chem. Phys. Discuss., https://doi.org/10.5194/acp-2018-608
Manuscript under review for journal Atmos. Chem. Phys.
Discussion started: 2 July 2018

Atmospheric Chemistry and Physics Discussions

Two years online measurement of fine particulate nitrate in western Yangtze River Delta: Influences of thermodynamics and N_2O_5 hydrolysis

Peng Sun[1], Wei Nie[1,2,*], Xuguang Chi[1,2], Yuning Xie[1], Xin Huang[1,2], Zheng Xu[1,2], Ximeng Qi[1,2], , Zhengning Xu[1], Lei Wang[1], Tianyi Wang[1], Qi Zhang[3], and Aijun Ding[1,2,*]

[1]Joint International Research Laboratory of Atmospheric and Earth System Science s, and School of Atmospheric Sciences, Nanjing University, Nanjing, 210023, China
[2]Jiangsu Provincial Collaborative Innovation Center of Climate Change, Nanjing, 210023, China
[3]Department of Environmental Toxicology, University of California, Davis, CA 95616, USA

Correspondence: Wei Nie (niewei@nju.edu.cn) and Aijun Ding (dingaj@nju.edu.cn)

Abstract.

Particulate nitrate contributes a large fraction of secondary aerosols. Despite understanding of its important role in regional air quality and global climate, long-term continuous measurements are rather limited in China. In this study, we conducted online measurement of $PM_{2.5}$ nitrate for two years from March 2014 to February 2016 using the Monitor for Aerosols and Gases in ambient Air (MARGA) in the western Yangtze River Delta (YRD), eastern China, and investigate the main factors that influenced its temporal variations and formation pathways. Compared to other sites in China, an overall high concentration of particulate nitrate was observed with a mean value of 15.8 μg m^{-3} (0.5 to 92.6 μg m^{-3}). Nitrate on average accounted for 32% of the total mass of water-soluble ions and the proportion increased with PM loading, indicating that nitrate is a major driver of haze pollution episodes in this region. Sufficient ammonia drove most nitrate into the particle phase in the form of ammonium nitrate. A typical seasonal cycle of nitrate was observed with the concentrations in winter on average two times higher than those in summer mainly due to different meteorological conditions. In summer, the diurnal variation of particulate nitrate was determined by the thermodynamic equilibrium, resulting in a much lower concentration during daytime despite of a considerable photochemical production. Air masses from polluted YRD

Atmos. Chem. Phys. Discuss., https://doi.org/10.5194/acp-2018-608
Manuscript under review for journal Atmos. Chem. Phys.
Discussion started: 2 July 2018

Atmospheric Chemistry and Physics Discussions

and biomass burning region contributed to the high nitrate concentration during summer. In winter, particulate nitrate didn't reveal an evident diurnal variation. Regional transport from northern China played an important role in enhancing nitrate concentration. Eighteen nitrate episodes were selected to understand the processes that drive the formation of high concentration of nitrate. Rapid nitrate formation was observed during the pre-episode (the day before nitrate episode day) nights, and dominated the increase of total water-soluble ions. Calculated nitrate from N_2O_5 hydrolysis was highly correlated to and accounted for 80 percent of the observed nitrate, suggesting that N_2O_5 hydrolysis was a major contributor to the nitrate episodes. Our results suggested that rapid formation of nitrate could be a main cause for extreme aerosol pollution events in YRD during winter, and illustrated the urgent needs to control the NO_x emission.

1. Introduction

Particulate nitrate (NO_3^-), as a major aerosol component in the atmosphere, reduces atmospheric visibility (Charlson and Heintzenberg, 1995), influences human health, alters radiative forcing and hence influences regional even global climate (IPCC, 2013). Compared to the sulfate, nitrate has a larger scattering albedo under low RH conditions that cause a stronger influence on visibility (Lei and Wuebbles, 2013). High concentration of particulate nitrate had been demonstrated to be one of the major reasons for the frequent occurrence of haze episodes in China (Wang and Zhang, 2009; Wen et al., 2015; Wang et al., 2017). In recent decades, Chinese government started to control emissions of air pollutants with special effort on the SO_2 reduction. This resulted in a remarkable decrease of ambient SO_2 and sulfate concentrations after 2006 (van der A et al., 2017; Wang et al., 2017). However, particulate nitrate, as well as its proportion in PM, showed increasing trends due to the strong emission of nitrogen oxides (NO_x) (Lei and Wuebbles, 2013; Yang et al., 2017).

Particulate nitrate can be formed from multiple pathways. Gas phase reaction of NO_2 and OH radical is one major pathway to form nitric acid (HNO_3) (Calvert and

Atmos. Chem. Phys. Discuss., https://doi.org/10.5194/acp-2018-608
Manuscript under review for journal Atmos. Chem. Phys.
Discussion started: 2 July 2018

Atmospheric Chemistry and Physics Discussions

Stockwell, 1983), which subsequently reacts with ammonia (NH_3) to produce ammonium nitrate (NH_4NO_3). As typical photochemical processes, these reactions dominate daytime nitrate formation, and have been widely investigated in both field and modelling studies (Sharma et al., 2007; Petetin et al., 2016). Heterogeneous uptake of the photochemical formed nitric acid by alkali compounds, e.g. dust and sea salt particles, is also a considerable pathway to form nitrate in some regions (Bian et al., 2014). During nighttime, the hydrolysis of dinitrogen pentoxide (N_2O_5) is believed to be the dominate pathway to form particulate nitrate. N_2O_5 is an important reactive nitrogen species in the polluted troposphere (Brown and Dube., 2007; Osthoff et al., 2006; Li et al., 2017; Brown et al., 2003; Brown and Stutz, 2012) and accumulates via the reversible reaction between NO_2 and NO_3 radical produced from the reaction of NO_2 with O_3. Due to the rapid photolysis of NO_3 radical, N_2O_5 concentration during daytime is rather low that its contribution to nitrate can be ignored. While during nighttime, N_2O_5 concentration can be up to ppb level, and form nitric acid by reaction with water vapor, or particulate nitrate directly by heterogeneous hydrolysis on the wet surface (Wang et al., 2017; Wen et al., 2018; Thornton et al., 2003). In China, the pollution episodes with high nitrate concentrations mostly occurred in winter, during which the photochemical production of nitrate should be overall weak. N_2O_5 hydrolysis thus has the potential to be the crucial contributor, however there is still a lack of observational evidences.

Collecting particulate matter on a filter with subsequent ion chromatography analysis in laboratories is the conventional method to measure the concentration of particulate nitrate. The un-denude filter pack system, which is most-widely used, can suffer from both positive artifacts by absorbing gas-phase nitric acid, and negative artifacts by the evaporation of ammonium nitrate (Nie et al., 2010; Pathak and Wu, 2009; Wang et al., 2010). A denuder system can minimize these sampling artifacts by adding denuders to remove the interfering gases and back-up filters to collect the evaporated vapers (John et al., 1988). However, the operation of such a denuder system

is super labor intensive and thus not widely used. In addition, the poor time-resolution of filter-based measurement can limit our understanding on the formation and chemical evolution of the particulate nitrate. To overcome these shortcomings, several continuous and semi-continuous techniques have been developed based on an online denude-IC system (e.g. the ambient ion monitor (AIM), the gas and aerosol collector ion chromatography (GAC-IC), the particle-into-liquid sample ion chromatography (PILS-IC) and MARGA), as well as mass spectrometry (e.g. AMS). Pathak et al. (2011) applied an AIM instrument in Beijing and Shanghai for one month and found that the heterogeneous hydrolysis of N_2O_5 contributed 50%~100% of the nighttime nitrate formation. Xue et al. (2013) deployed a PILS-IC system in Hong Kong for less than a month and showed a more active nitrate formation during PM episode than normal days. Wen et al. (2015) used a MARGA instrument in Yucheng, North China during summer and emphasized the important roles of O_3 and NH_3 on nitrate formation. Yang et al. (2017) carried out field observation with ACSM in Beijing for half a month and pointed out the importance of aerosol nitrate in haze formation. However, despite of an increasing number of studies using online techniques, continuous measurements with more than one-year period are still very limited.

The Yangtze River Delta (YRD) located in the eastern China, with megacities including Shanghai, Nanjing and Suzhou etc., has suffered from heavy particulate matter pollution and photochemical pollution (Ding et al., 2013bc; Wang et al., 2016bc; Wang et al., 2016a). Previous studies indicated an important role of nitrate in the pollution episodes (Hua et al., 2015; Du et al., 2011; Yang et al., 2017). For example, Zhang et al. (2015) carried out an observation with ACSM in urban Nanjing during summer and autumn, and found nitrate and organic aerosols dominated the PM_1 composition. Shi et all. (2014) used MARGA instrument in Shanghai for months and found and increasing contribution of nitrate to PM_1 mass during pollution periods. Wang et al. (2016b) reported temporal variation and transport of $PM_{2.5}$ water soluble ions, including nitrate, in an urban site in Shanghai based on three-year continuous

measurement using MARGA. However, detailed investigation on the possible mechanisms governing nitrate behaviors during haze pollution is still rare.

In this study, we present a 2-year continuous measurement of particulate nitrate using MARGA at a rural site in Nanjing, a megacity in the western YRD region, with the target to get a comprehensive understanding of particulate nitrate behaviors and investigate the processes affecting nitrate in haze episodes. We first conducted general statistical analysis of particulate nitrate and characterized seasonal variation and diurnal pattern. A thermodynamic model was then applied to investigate the gas-particle partition of nitrate. The influence of air masses was also investigated by conducting backward Lagrangian dispersion modelling. Finally, we selected eighteen nitrate episodes and investigated the main processes influencing their evolution.

2. Methodology

2.1. Sample site and instrumentation

The SORPES station (118°57′E, 32°07′N) was located on the top of a small hill (40 m above sea level) in the Xianlin campus of Nanjing University located in the outskirts of Nanjing, China. The station is an ideal receptor of air masses from the YRD with little influence of local emissions and urban pollution from Nanjing. Detailed description can be found in previous studies (Ding et al., 2013c; Ding et al., 2016a).

The measurement was conducted from March 2014 to Feb 2016. Hourly concentrations of water soluble gases of HCl, HNO_3, HONO, SO_2 and NH_3, and water-soluble ions in $PM_{2.5}$, including Cl^-, NO_3^-, SO_4^{2-}, NH_4^+, Na^+, K^+, Ca^{2+}, and Mg^{2+}, were measured with a Monitor for Aerosols and Gases in ambient Air (MARGA, designed and manufactured by Applikon Analytical B.V., the Netherlands) employed in connection with a Thermo $PM_{2.5}$ cyclone inlet. The sampling system was comprised of two parts: A Wet Rotating Denuder for gases and a Steam Jet Aerosol Collector for aerosols, working at an air flow of 1 m^3 h^{-1} (ten Brink et al., 2007; Rumsey et al., 2014). After each hour's collection, the samples were analyzed using ion chromatography. The instrument was calibrated on an hourly basis using internal standard liquid (bromide

Atmos. Chem. Phys. Discuss., https://doi.org/10.5194/acp-2018-608
Manuscript under review for journal Atmos. Chem. Phys.
Discussion started: 2 July 2018

Atmospheric Chemistry and Physics Discussions

lithium), ensuring a stable and reliable ion chromatograph. Concentrations of all aerosol ions and gases have a precision of 0.001μg m^{-3} (Xie et al., 2015). The $PM_{2.5}$ ion dataset from the MARGA provided more than 15000 hourly samples over the 24 months of measurements considering points where NO_3^-, NH_4^+ and SO_4^{2-} were all available. Trace gases (i.e., O_3, SO_2, NO_x, NO) and $PM_{2.5}$ mass concentrations were also measured at SORPES (Ding et al., 2013c; Nie et al., 2015; Ding et al., 2016a), together with meteorological data including wind speed/direction, temperature, and relative humidity.

2.2. Thermodynamic constants and ISORROPIA II

Formation of ammonium nitrate involves an equilibrium reaction between the gas phase NH_3 and HNO_3, and particle phase NH_4NO_3. The gas-to-particle partitioning is temperature dependent, and the equilibrium constant can be calculated as follows (units $mol^2kg^{-2}atm^{-2}$) (Sun et al., 2011; Seinfeld and Pandis, 2006):

$$K=k_{298}\, exp(a(298/T-1) +b[1+ln(298/T)-298/T]) \quad (1)$$

$$K_{298}=3.5\times10^{16}(atm^{-2}),\ a=75.11,\ b=-13.5. \quad (2)$$

The dissociation constant, K_p (T), is the value to examine the product of the partial pressures of NH_3 and HNO_3 in ideal equilibrium state at a specific temperature and can be calculated as follows (units: ppb^2) (Sharma et al., 2007; Seinfeld and Pandis, 2006):

$$ln\ K_p= 84.6-24220/T-6.4ln(T/298)\ (T \text{ is temperature in Kelvin}) \quad (3)$$

Note that the constant is quite sensitive to temperature changes. Lower values of K_p correspond to lower equilibrium values of the NH_3 and HNO_3 gas phase concentrations, shifting the equilibrium of the system toward the aerosol phase.

ISORROPIA II (available at http://isorropia.eas.gatech.edu/) is a thermodynamic model used commonly in inorganic aerosol research (Fountoukis and Nenes, 2007). To analyze gas-into-particulate pathway for nitrate formation, HNO_3 was modeled with ISORROPIA II run in forward model iteratively (Pusede et al., 2016; Fountoukis and Nenes, 2007). ISORROPIA II was initialized as $[NO_3^-+HNO_3]_{total} = [NO_3^-]_{aerosol}$. Calculated HNO_3(g) was added back to $[NO_3^-+HNO_3]$, while we always use $[NH_4^+{}_{aerosol}+NH_3(g)]$ as input total ammonium. ISORROPIA II was solved iteratively

until output NO_3^- changed by < 2% by mass. The phase state was set as metastable. We assume that gases and aerosol are in equilibrium, that aerosols are homogeneous and internally mixed, and that unaccounted-for factors do not influence the thermodynamics of system (Vayenas et al., 2005).

2.3. Lagrangian Dispersion Modeling

To help understand the influence of air masses, backward Lagrangian particulate dispersion modeling (LPDM) was carried out based on a method developed and evaluated by Ding (Ding et al., 2013a). The LPDM was conducted using the Hybrid Single-Particulate Lagrangian Integrated Trajectory model developed in the Air Resource Laboratory (ARL) of the National Oceanic and Atmospheric Administration using the ARL format Global Data Assimilation System data. The model calculates the position of particulates by mean wind and a turbulence transport component after they are released at the source point for a backward simulation. For each hour, 3000 particulates were released at 100 m altitude over the site and were traced backward for a 3-day period. The hourly position of each particulate was calculated using a 3-D particulate, i.e., horizontal and vertical, method. The residence time at 100 m altitude, i.e., foot-print "retroplume", which represents the distribution of the surface probability or residence time of the simulated air mass, was used to understand the contribution from potential source regions (Ding et al., 2013ac; Shen et al., 2018).

2.4. Steady-state predictions

Based on their short lifetimes, the concentrations of the NO_3 radical and N_2O_5 can be predicted by steady-state calculations due to lack of measurement data (Osthoff et al., 2006). The formation and loss of N_2O_5 associated with a series of chemical reactions are listed in Table 1. For the heterogeneous processes, we used 0.004 and 0.03 as the uptake coefficients of the NO_3 radical and N_2O_5 (γNO_3 and γN_2O_5), respectively (Aldener et al., 2006; Wen et al., 2015; Knopf et al., 2011; Brown et al., 2006). Due to the lack of VOC measurement data, the total reaction rates of NO_3 with VOCs were assumed to be equal to the NO_3 loss rate caused by the heterogeneous hydrolysis of

N_2O_5 (Aldener et al., 2006; Wen et al., 2015). The corresponding rate constant can be found in Master Chemical Mechanism (MCM version 3.1, http://mcm.leeds.ac.uk/MCM/).

3. Results and discussion

3.1. Overall results

A MARGA was deployed to continuously measure the eight water-soluble ions (WSI) of $PM_{2.5}$ and several gas-phase species from March 2014 to February 2016 with the time resolution of 1-hour. Nitrate (NO_3^-), sulfate (SO_4^{2-}) and ammonium (NH_4^+) were the major components with the two-year averaged concentrations of 15.8 (±13.4),15.3 (±10.6) and 10.4 (±7.6) μg m^{-3}, respectively. In the present study, we focused on nitrate, and discussed the temporal variation and its association with physicochemical processes. The concentration of $PM_{2.5}$ nitrate changed largely from 0.5 to 92.6 μg m^{-3} during the measurement period, and accounted for 3% to 58% of total WSI (=45.7 + 30μg m^{-3}). The highest hourly nitrate concentration occurred on December 23, 2015 together with high concentrations of sulfate (65.5 μg m^{-3}), and ammonium (56.8 μg m^{-3}). Heavy haze episode like this occurred at our site frequently during winter. To understand the influence of wind on nitrate concentration, the wind rose plot is given in Fig. S1. The prevailing winds at the SORPES station were from northeast and east during the two-year observation period. Particulate nitrate tended to accumulate or formed under stagnant condition of low wind speed. The wind from west and east can lead to a higher nitrate concentration and also other aerosol components (Ding et al., 2013bc; Shen et al., 2018), which may be associated with air masses from biomass burning region and the city clusters of YRD.

To get an overall picture of nitrate distribution in developed region of costal China, we reviewed results from available nitrate measurements in three most polluted regions of North China Plain (NCP), YRD and Pearl River Delta (PRD), and summarized their concentration, sampling sites and measurement techniques in Fig. 1. Measurements in summer and winter were separated due to the large seasonal difference of particulate

nitrate. Despite that these measurements were from various measurement techniques, the results still can give us some insights about the differences in spatial and temporal scales. First, particulate nitrate generally showed the highest concentration in NCP and followed by YRD and PRD. This was in consistence with the spatial distribution of NO_2 – a major gas precursor of nitrate. Second, evident seasonal variations can be observed at all three regions with much higher concentrations in winter. Third, there was an overall increase trend of particulate nitrate in NCP and YRD in the past decade, especially that during summertime. Nevertheless, particulate nitrate in PRD revealed an overall decreasing trend. Compared to these previous studies, the nitrate concentration during summertime at SORPES station was lower than that in NCP, but higher than that in YRD and PRD cities. In terms of wintertime, nitrate concentration at SORPES station was slightly lower than that in NCP, comparable with that in YRD, and higher than that in PRD.

Fig. 2 illustrates the occurrence frequency of the loading of particle matter in different concentration range, and the changes of nitrate proportion along with the PM loading. Noting that the PM loading here was indicated by the mass of total WSI. The highest frequency of WSI concentrations occurred in a range of 20-40 μg m^{-3}, and gradually decreased with the increasing of concentration. Heavy PM pollution with WSI concentrations higher than 100 μg m^{-3} occurred during more than 5% of the time during this study. The contribution of nitrate to total WSI increased with the PM loading, ranging from ~25% with WSI concentration lower than 20 μg m^{-3} to ~ 40% when WSI was higher than 140 μg m^{-3}. These results suggested that nitrate was a major driver of haze episodes with high PM peaks in this region.

Fig. 3a shows the scatter plot of particulate nitrate and total WSI. They overall correlated to each other with correlation coefficient R = 0.92, and nitrate accounted for 32% of the total WSI. Air temperature greatly affected the contribution of nitrate to total WSI. Its proportion can be up to 58% at around 0 °C and only 3% at the temperature higher than 30 °C, indicating an important role of thermodynamic equilibrium in nitrate

concentration. We further investigated the neutralization extent of sulfate and nitrate by ammonium (Fig. 3b). Ammonium was overall enough to neutralize both sulfate and nitrate, suggesting that the particulate nitrate mostly existed as ammonium nitrate at SORPES station, contrasts with some ammonia poor regions, where excess NH_4^+ defined as $([NH_4^+]/[SO_4^{2-}]-1.5) \times [SO_4^{2-}]$ played an important role in the formation of particulate nitrate (Pathak and Wu, 2009). Evident seasonal difference can be observed for the molar ratio of ammonium to the sum of sulfate and nitrate. In spring and early summer, a fraction of the particulate nitrate is present in the forms of $Ca(NO_3)_2$ and KNO_3; while in winter, considerable chloride would consume some ammonium to form NH_4Cl.

3.2. Characteristics of fine particular nitrate in different seasons.

3.2.1. Seasonal pattern and its main causes

Fig. 4 shows the composite seasonal pattern of NO_x, $PM_{2.5}$ nitrate, sulfate and the ratio of nitrate to sulfate during the 2-year period at SORPES station. Similar to the previous studies (Griffith et al., 2015), a typical seasonal variation was observed for particulate nitrate (and its ratio to sulfate, i.e. NO_3^-/SO_4^{2-}), with a maximum value of 23.7 μg m^{-3} (140%) in January, and a minimum of 8.4 μg m^{-3} (66%) in August and September. Particulate sulfate revealed a bimodal pattern with high concentrations occurred in January and June, respectively. The low value of particulate nitrate during summer can be generally explained by the higher temperature, higher and unstable boundary layer and relative clean air masses induced by summer monsoon (Ding et al., 2013c) despite of the increased photochemical formation. In opposite, the high values during winter were generally due to the lower temperature, lower and stable boundary layer and relative stronger continental outflow from the North China where anthropogenic emission was relatively high due to heating in winter (Ding et al., 2013c). Different chemical processes that affects nitrate concentrations between summer and winter will be discussed later. NO_x, the major precursor, tracked the changes of particulate nitrate commendably, except for that during February and June. In addition, a secondary peak

of particulate nitrate can be observed during June, which can be explained as the influence from agricultural burning in eastern China (Ding et al., 2013bc; Xie et al., 2015; Shen et al., 2018). The concentrations of Potassium, a biomass burning tracer in this region (Ding et al., 2013b; Xie et al., 2015), clearly showed a consistent peak (Fig. S2) with both particulate nitrate and sulfate, as well as the discrepancy of NO_x and nitrate concentrations (Ding et al., 2013b; Xie et al., 2015; Nie et al., 2015) shown in Fig. 4. While in February, the nitrate concentration didn't show concurrent decrease in NO_x during the Chinese Spring Festival (Ding et al., 2013c). It might suggest that local emissions were not the major contributor to the particulate nitrate observed in winter.

Thermodynamics is an important factor influencing the formation and partitioning of nitrate. Here, we calculated the dissociation constant (K_p) to evaluate whether ambient conditions favored the formation of aerosol NH_4NO_3. The hourly NH_3 concentration was measured by MARGA and HNO_3 was calculated by ISORROPIA II. As showed in Fig. 5, the product of [NH_3(g)] and [HNO_3(g)] for most ambient samples during summer was lower than the calculated K_p, suggesting ambient condition during summer at SORPES favored to evaporate ammonium nitrate to gas phase NH_3 and HNO_3 (Fig. 5a). In contranst, ambient conditions during winter favored to form particulate nitrate in most cases (Fig. 5b). This study also shows the similar result with the study reported in the Kanpur, India (Sharma et al., 2007).

3.2.2. Diurnal cycles during summer and winter

In Fig. 6, we show the averaged diurnal variations of particulate nitrate, nitrogen dioxide, nitric acid, equilibrium constant (K), air temperature and RH during summer and winter during the two years. Nitric acid was calculated by ISORROPIA II. In summer (Fig. 6a), the fine particulate nitrate showed a typical diurnal cycle that the maximum concentration occurred at 7:00 with the average concentration of 16.5 μg m^{-3} and minimum value at 14:00 (7.2 μg m^{-3}). This summertime diurnal pattern of nitrate is very similar with the findings in Shandong (Wen et al., 2015) and New York (Sun et al., 2011). However, it is quite different from the findings in Hong Kong (Griffith et al.,

2015), where nitrate concentration peaks in the daytime in summer. Ambient temperature and the development of boundary layer are the major drivers to the observed diurnal variation of particulate nitrate, and high temperature and high boundary layer during daytime prefer to evaporate and dilute the particulate nitrate (Zhang et al., 2015a; Ding et al., 2016). Nitric acid, which accounted for 20% of the total nitrate [NO_3^-+HNO_3], revealed its high concentration (around 2 ppb) in the noontime (12:00-15:00). NO_2, the precursor of nitrate, showed a peak concentration of 18.2 ppb at 21:00, and remained at a high level during the whole night. Equilibrium constant, *K*, was calculated to understand the influence of gas-to-particulate partitioning on the observed diurnal variation of particulate nitrate (Sun et al., 2011). As showed in Fig. 6a, *K* was highly correlated to particulate nitrate, suggesting the thermodynamic is the major factor influencing the diurnal variation of particle nitrate during summer.

In winter, the diurnal variation is small with a considerable peak appeared at around 10:00 AM. Compared to that in summer, K showed similar diurnal variation, but not correlated to particulate nitrate, indicating factors other than the control of temperature. The observed peak at late morning was probably due to downward mixing from the residual layer where particulate nitrate was formed aloft during the night and brought to the surface after sunrise following the breakup of the boundary layer (Brown and Dube., 2007; Young et al., 2016; Pusede et al., 2016). Direct vertical observations are needed to further investigate this issue.

To further investigate factors influencing the nitrate behaviors other than thermodynamics, ISORROPIA II was used to simulate the diurnal variation of nitrate. Hourly concentrations of all species (both gas and aerosol phase species) at 00:00 were used as the initial value of each specific day. Hourly data of temperature and relative humidity were used as the input data to constrain the model. The ISORROPIA II model was set as forward mode and metastable phase state. The calculated diurnal variations were showed in Fig. 7 together with the observed results.

The differences between the calculation and the observation could be attributed to:

(1) the development of boundary layer, (2) the dry deposition of nitric acid, and (3) chemical processes, which has not been considered yet in the model. As shown in Fig. 7a, the overall diurnal pattern of nitrate in summer is well captured by the model except for 3 periods. The differences after midnight are likely caused by the effect of boundary layer height and some chemical processes. Faster increase of model nitrate after 18:00 was attributed to lack of dry deposition of nitric acid in the model. During noontime the observed nitrate concentration was expected to be lower than the calculated value because of the development of boundary layer and stronger dry deposition of nitric acid associated with stronger turbulence mixing, which were ignored in the model. However, in contrast, the observation was considerably higher than the calculated value. It indicates a strong production of nitrate via photochemical processes in summer. Fig.7c shows that the difference between calculated and observed nitrate concentration was in good correlation with the production of NO_2 and solar radiation, a proxy for production rate of nitric acid (Zhang et al., 2005; Young et al., 2016), further suggesting that photo-oxidation of NO_2 is an important source of nitrate during summer, even though the thermodynamic equilibrium is the dominate factor controlling the diurnal cycle. Wen et al. (2018) also demonstrated that photochemical production of nitric acid is a major contributor to daytime nitrate increase during summer in North China Plain. In winter, the influence of thermodynamics is small since the low temperature. The peaks in the morning may be caused by the mixing down of a residual layer enriched of nitrate as mentioned above, while the decline during the afternoon are supposed to be the result of dilution associated with the boundary layer development.

3.2.3 Influence of air masses transport

Meteorological processes play a key role in air masses long-range transport and local accumulation (Ding et al., 2013ac; Zhang et al., 2016; Ding et al, 2016b). In order to investigate the influence of air masses transport on nitrate concentrations, Lagrangian dispersion modeling was conducted for the sampling days with the highest and lowest 25^{th} percent nitrate concentration in summer and winter, respectively (Ding et al.,

2013a). Fig. 8 shows the retroplumes, i.e. footprint at an altitude of 100 m, of the selected days during summer and winter, respectively. In summer, high concentrations of nitrate tended to accompany with the air masses from west of Nanjing (mostly Anhui province) and Yangtze River Delta (Suzhou-Shanghai city clusters and North Zhejiang province) (Fig. 8a). YRD is a high NO_x emission region (Fig. 1), air masses from which could bring high concentration of NO_x to enhance the nitrate concentration at SORPES station. Biomass burning is the possible cause of the high nitrate loading with air mass from the west of Nanjing (Fig. S3). In winter, regional transport from northern China played an important role in enhancing nitrate concentrations. As shown in Fig. 8c, a large part of air masses for the highest 25% sampling days was from North China Plain, which has the strongest NO_x emission in China (Fig. 1). It should be noted here that the longer lifetime of particulate nitrate during winter might be the main cause to promote the contribution of regional transport to the observed nitrate at SORPES. In contrast, the lowest 25% sampling days during winter tended to be accompanied with the air mass from Nanjing local and marine areas.

3.3. Contribution of N_2O_5 hydrolysis to nitrate episodes

Similar to findings from previous studies (Zhang et al., 2015c), nitrate was found to increase significantly during this study and become the largest contributor of $PM_{2.5}$ during the haze episodes (Fig. 2). Generally, these pollution episodes mainly occurred in winter (Fig. 3a and Fig. 4), during which the photochemical production of nitric acid should be weak. N_2O_5 hydrolysis was thus proposed to be a potential important formation pathway. Here we investigated the nitrate episodes in detail and discussed their relationship to the N_2O_5 hydrolysis during the nights before.

In Fig. 9, we show a typical case of nitrate episodes from 30 November to 2 December, 2015. Fast nitrate formation was observed, which was likely caused by hydrolysis of N_2O_5. Nitrate increased significantly from 20.3 μg m^{-3} at 18:00 of 30 November to 63 μg m^{-3} at 6:00 of 1 December, 2015. The ratio of nitrate to $PM_{2.5}$ also exhibited a large increase from 25% at 18:00 to 38% at 06:00. In contrast, other $PM_{2.5}$

components, e.g. sulfate and black carbon, showed only slight increases. High concentration of NO_2, considerable level of O_3 and extremely low concentration of NO provided a favorable condition towards forming NO_3 and N_2O_5 (Brown et al., 2003). The meteorological conditions during these 12 hours were stable with low wind speed and high relative humidity, which, combined with the relatively high concentration of PM, would promote the hydrolysis of N_2O_5 (Riemer, 2003).

N_2O_5 concentrations were calculated by using steady-state expressions (Osthoff et al., 2006;Wang et al., 2014;Wen et al., 2015), and the result was shown in Fig. 9. The calculated N_2O_5 exhibited a much higher concentration during the night of 30 November compared to the days before and after. Particulate nitrate formed from N_2O_5 hydrolysis was then computed during the 12-hour period. Nitrate concentration at 18:00 of 30 November, 2015 (20 μg m^{-3}) was selected as the initial value, and 31 μg m^{-3} of particulate nitrate was produced in the following 12 hours, suggesting that approximate 80% of increased particulate nitrate can be attributed to the hydrolysis of N_2O_5 in this case.

To further understand the contribution of N_2O_5 hydrolysis, sampling days with daily-averaged nitrate concentration exceeding the mean plus twice the standard deviation were selected as the nitrate episode days. In total, 18 episode-days were selected during the 2-year measurement, with 16 days in winter and the other 2 days in biomass burning season. In Fig. 10, we presented the averaged diurnal pattern of particulate nitrate and its related parameters on the 18 selected episode and pre-episode days. For the episode days, particulate nitrate revealed a similar diurnal pattern as that of the whole winter (Fig. 6). Nitrate maintained a high concentration during the whole day with a small peak around 10:00 in the morning. However, for the pre-episode days, a clear build-up of nitrate can be observed, especially during the nighttime from 17:00 of the pre-episode days to 1:00 of the episode days (as marked in Fig. 10). The average increment of ammonium nitrate has exceeded 24 μg m^{-3} during this 9-hour period of the pre-episode nighttime. The total WIS also increased during this period, which was

mostly attributed to ammonium nitrate (almost 90%) and resulted in an evident increase of the ratio of nitrate to total WSI. Compared to nitrate, black carbon, a tracer of primary emissions, showed little change during the pre-episode day. The retroplume showed in Fig. S4 suggested that the air masses arrived at the SORPES station on the pre-episode and episode days were almost the same. These results suggest that secondary formation other than accumulation was the major contributor to the observed increase of particulate nitrate.

Since the observed nitrate formation mostly occurred during the nighttime of pre-episode days when the photochemical production of nitric acid would be largely suppressed, N_2O_5 hydrolysis is thus believed to be the major contributor. As showed in Fig. 10, compared to those during episode days, NO_2 concentration was comparable, but O_3 concentration was higher during pre-episode days. This resulted in a higher production rate of N_2O_5 proxy ($NO_2 \times O_3$) in pre-episode days, and favored formation of nitrate from the hydrolysis of N_2O_5. We further calculated the contribution of N_2O_5 hydrolysis to nitrate formation during the periods from 17:00 to 23:00 of each pre-episode day (excluding 2 windy days). A good correlation (R=0.8) was observed between the calculated nitrate and observed nitrate (Fig. 11), with the slope of 0.8, indicating most of the observed nitrate formation during nitrate episodes were attributed to the hydrolysis of N_2O_5.

4. Summary and Conclusion

Online measurements of fine particulate nitrate along with trace gases and $PM_{2.5}$ mass concentrations were conducted for two years from March 2014 to February 2016 using a MARGA at SORPES station, a rural receptor site in the Yangtze River Delta, eastern China. Hourly nitrate concentration varied from 0.5 μg m^{-3} to 92.6 μg m^{-3}, with an averaged value of 15.8 μg m^{-3}, which was generally higher than the measurement at the sites in YRD and PRD, but lower than that at the sites in North China Plain. The contribution of nitrate to total WSI increased from 25% with WSI concentration lower than 20 μg m^{-3}, to 40% when WSI was higher than 140 μg m^{-3}, suggesting a major

449 driver of nitrate to the aerosol pollution in YRD. NH_3 is enough to neutralize the acidic
450 compounds of aerosol, ammonium nitrate was thus the predominate form of the
451 observed particulate nitrate. A clear seasonal variation of nitrate was observed with
452 peak value in January and December and lowest value in August and September.
453 Biomass burning plumes contributed the nitrate concentration evidently and resulted in
454 a secondary peak during June. In summer, thermodynamic equilibrium was the major
455 factor influencing the diurnal variation of nitrate, and resulted in a much lower
456 concentration at noontime. Nevertheless, the observed nitrate at noontime was
457 considerably higher than the value predicted by ISORROPIA II model, indicating a
458 strong production of nitrate by the photo-oxidation of NO_2. Air masses from YRD and
459 biomass burning region were corresponded to the high nitrate concentrations during
460 summer. In winter, the diurnal variation of nitrate was weak. Regional transport from
461 North China Plain contributed largely to the observed high nitrate concentrations.
462 Nitrate episodes, defined as daily-averaged concentration exceeding the mean
463 value plus twice the standard deviation, were further investigated to understand the
464 chemical processes towards forming particulate nitrate and their contribution to the
465 pollution episodes. A clear build-up of nitrate can be observed during the pre-episode
466 night, and dominated the increase of total WSI. N_2O_5 hydrolysis was demonstrated to
467 contribute 80% of the observed nitrate formation, suggesting its critical role in an
468 aerosol pollution episode. In view of the significant emission of NO, which is the main
469 sink of N_2O_5 during night, stronger production of N_2O_5 is expected at the upper
470 boundary layer, e.g. residual layer, and contribute to the nitrate formation in the entire
471 boundary layer. In summary, our study provides evidence that particulate nitrate
472 especially that formed from N_2O_5 hydrolysis is a crucial contributor to the aerosol
473 pollution episodes in eastern China.

474 *Data availability*. The GDAS data used in the HYSPLIT calculation can be acquired
475 from ftp://arlftp.arlhq.noaa.gov/pub/archives/gdas1. Measurement data at SORPES,

including aerosol data and relevant trace gases as well as meteorological data, are available upon request from the corresponding author before the SORPES database is opened publicly.

Acknowledgements. The research was supported by National Key Research & Development Program of China (2016YFC0200500) and National Science Foundation of China (41725020, 91544231, 91644218, 41422504, 91744311, 41675145).

References

Aldener, M., Brown, S. S., Stark, H., Williams, E. J., Lerner, B. M., Kuster, W. C., Goldan, P. D., Quinn, P. K., Bates, T. S., Fehsenfeld, F. C., and Ravishankara, A. R.: Reactivity and loss mechanisms of NO3 and N2O5 in a polluted marine environment: Results from in situ measurements during New England Air Quality Study 2002, J Geophys Res-Atmos, 111, 2006.

Bian, Q., Huang, X. H. H., and Yu, J. Z.: One-year observations of size distribution characteristics of major aerosol constituents at a coastal receptor site in Hong Kong – Part 1: Inorganic ions and oxalate, Atmospheric Chemistry and Physics, 14, 9013-9027, 10.5194/acp-14-9013-2014, 2014.

Brown, S. S., Stark, H., Ryerson, T. B., Williams, E. J., Nicks, D. K., Trainer, M., Fehsenfeld, F. C., and Ravishankara, A. R.: Nitrogen oxides in the nocturnal boundary layer: Simultaneous in situ measurements of NO3, N2O5, NO2, NO, and O-3, J Geophys Res-Atmos, 108, 2003.

Brown, S. S., Ryerson, T. B., Wollny, A. G., Brock, C. A., Peltier, R., Sullivan, A. P., Weber, R. J., Dube, W. P., Trainer, M., Meagher, J. F., Fehsenfeld, F. C., and Ravishankara, A. R.: Variability in nocturnal nitrogen oxide processing and its role in regional air quality, Science, 311, 67-70, 2006.

Brown, S. S., and W.P.Dube.: High resolution vertical distributions of NO_3 and N_2O_5 through the nocturnal boundary layer, Atmospheric Chemistry and Physics, 7, 139-149, 2007.

Brown, S. S., and Stutz, J.: Nighttime radical observations and chemistry, Chem Soc Rev, 41, 6405-6447, 2012.

Calvert, J. G., and Stockwell, W. R.: Acidic generation in the troposphere by gas phase chemistry, Environ. Sci. Technol., 17, 428-443, 1983.

Cao, J.-J., Shen, Z.-X., Chow, J. C., Watson, J. G., Lee, S.-C., Tie, X.-X., Ho, K.-F., Wang, G.-H., and Han, Y.-M.: Winter and Summer PM2.5 Chemical Compositions in Fourteen Chinese Cities, Journal of the Air & Waste Management Association, 62, 1214-1226, 10.1080/10962247.2012.701193, 2012.

Charlson, R., and Heintzenberg, J.: Aerosol Forcing of Climate Environmental Sciences Research Report, 1995.

508 Ding, A., Wang, T., and Fu, C.: Transport characteristics and origins of carbon monoxide and ozone in
509 Hong Kong, South China, Journal of Geophysical Research: Atmospheres, 118, 9475-9488,
510 10.1002/jgrd.50714, 2013a.

511 Ding, A. J., Fu, C. B., Yang, X. Q., Sun, J. N., Petäjä, T., Kerminen, V. M., Wang, T., Xie, Y., Herrmann,
512 E., Zheng, L. F., Nie, W., Liu, Q., Wei, X. L., and Kulmala, M.: Intense atmospheric pollution
513 modifies weather: a case of mixed biomass burning with fossil fuel combustion pollution in eastern
514 China, Atmospheric Chemistry and Physics, 13, 10545-10554, 10.5194/acp-13-10545-2013, 2013b.

515 Ding, A. J., Fu, C. B., Yang, X. Q., Sun, J. N., Zheng, L. F., Xie, Y. N., Herrmann, E., Nie, W., Petäjä, T.,
516 Kerminen, V. M., and Kulmala, M.: Ozone and fine particle in the western Yangtze River Delta: an
517 overview of 1 yr data at the SORPES station, Atmospheric Chemistry and Physics, 13, 5813-5830,
518 10.5194/acp-13-5813-2013, 2013c.

519 Ding, A.J., Nie, W., Huang, X., Chi, X., Sun, J., Kerminen,V.-M., Xu, Z., Guo, W., Petäjä, T., Yang, X.,
520 Kulmala, M., and Fu, C.: Long-term observation of air pollution-weather/climate interactions at the
521 SORPES station: a review and outlook, Front. Environ. Sci. & Eng., 10, 5, 15, 2016a.

522 Ding, A.J., Huang, X., Nie, W., Sun, J.N., Kerminen, V.-M., Petaja, T., Su, H., Cheng, Y.F., Yang, X.-Q.,
523 Wang, M.H., Chi, X.G., Wang, J.P., Virkkula, A., Guo, W.D., Yuan, J., Wang, S.Y., Zhang, R.J., Wu,
524 Y.F., Song, Y., Zhu, T., Zilitinkevich, S., Kulmala, M., and Fu, C.B.: Ehanced haze pollution by
525 black carbon in megacities in China, Geophys. Res. Lett., 43, 6, 2873-2879, 2016b.

526 Du, H., Kong, L., Cheng, T., Chen, J., Du, J., Li, L., Xia, X., Leng, C., and Huang, G.: Insights into
527 summertime haze pollution events over Shanghai based on online water-soluble ionic composition
528 of aerosols, Atmospheric Environment, 45, 5131-5137, 10.1016/j.atmosenv.2011.06.027, 2011.

529 Fountoukis, C., and Nenes, A.: ISORROPIA II: a computationally efficient thermodynamic equilibrium
530 model for K+-Ca2+-Mg2+-Nh(4)(+)-Na+-SO42--NO3--Cl--H2O aerosols, Atmospheric Chemistry
531 and Physics, 7, 4639-4659, 2007.

532 Gao, X. M., Yang, L. X., Cheng, S. H., Gao, R., Zhou, Y., Xue, L. K., Shou, Y. P., Wang, J., Wang, X. F.,
533 Nie, W., Xu, P. J., and Wang, W. X.: Semi-continuous measurement of water-soluble ions in PM2.5
534 in Jinan, China: Temporal variations and source apportionments, Atmospheric Environment, 45,
535 6048-6056, 2011.

536 Griffith, S. M., Huang, X. H. H., Louie, P. K. K., and Yu, J. Z.: Characterizing the thermodynamic and
537 chemical composition factors controlling PM2.5 nitrate: Insights gained from two years of online
538 measurements in Hong Kong, Atmospheric Environment, 122, 864-875,
539 10.1016/j.atmosenv.2015.02.009, 2015.

540 He, L.-Y., Huang, X.-F., Xue, L., Hu, M., Lin, Y., Zheng, J., Zhang, R., and Zhang, Y.-H.: Submicron
541 aerosol analysis and organic source apportionment in an urban atmosphere in Pearl River Delta of
542 China using high-resolution aerosol mass spectrometry, Journal of Geophysical Research, 116,
543 10.1029/2010jd014566, 2011.

544 Hu, W., Hu, M., Hu, W.-W., Zheng, J., Chen, C., Wu, Y., and Guo, S.: Seasonal variations in high time-

resolved chemical compositions, sources, and evolution of atmospheric submicron aerosols in the megacity Beijing, Atmospheric Chemistry and Physics, 17, 9979-10000, 10.5194/acp-17-9979-2017, 2017.

Hua, Y., Cheng, Z., Wang, S., Jiang, J., Chen, D., Cai, S., Fu, X., Fu, Q., Chen, C., Xu, B., and Yu, J.: Characteristics and source apportionment of PM2.5 during a fall heavy haze episode in the Yangtze River Delta of China, Atmospheric Environment, 123, 380-391, 10.1016/j.atmosenv.2015.03.046, 2015.

John, W., Wall, S. M., and Ondo, J. L.: A New Method for Nitric-Acid and Nitrate Aerosol Measurement Using the Dichotomous Sampler, Atmospheric Environment, 22, 1627-1635, 1988.

Knopf, D. A., Forrester, S. M., and Slade, J. H.: Heterogeneous oxidation kinetics of organic biomass burning aerosol surrogates by O-3, NO2, N2O5, and NO3, Phys Chem Chem Phys, 13, 21050-21062, 2011

Lei, H., and Wuebbles, D. J.: Chemical competition in nitrate and sulfate formations and its effect on air quality, Atmospheric Environment, 80, 472-477, 10.1016/j.atmosenv.2013.08.036, 2013.

Li, H., Zhang, Q., Zhang, Q., Chen, C., Wang, L., Wei, Z., Zhou, S., Parworth, C., Zheng, B., Canonaco, F., Prévôt, A. S. H., Chen, P., Zhang, H., Wallington, T. J., and He, K.: Wintertime aerosol chemistry and haze evolution in an extremely polluted city of the North China Plain: significant contribution from coal and biomass combustion, Atmospheric Chemistry and Physics, 17, 4751-4768, 10.5194/acp-17-4751-2017, 2017.

Nie, W., Wang, T., Gao, X., Pathak, R. K., Wang, X., Gao, R., Zhang, Q., Yang, L., and Wang, W.: Comparison among filter-based, impactor-based and continuous techniques for measuring atmospheric fine sulfate and nitrate, Atmospheric Environment, 44, 4396-4403, 10.1016/j.atmosenv.2010.07.047, 2010.

Nie, W., Ding, A. J., Xie, Y. N., Xu, Z., Mao, H., Kerminen, V. M., Zheng, L. F., Qi, X. M., Huang, X., Yang, X. Q., Sun, J. N., Herrmann, E., Petäjä, T., Kulmala, M., and Fu, C. B.: Influence of biomass burning plumes on HONO chemistry in eastern China, Atmospheric Chemistry and Physics, 15, 1147-1159, 10.5194/acp-15-1147-2015, 2015.

Osthoff, H. D., Sommariva, R., Baynard, T., Pettersson, A., Williams, E. J., Lerner, B. M., Roberts, J. M., Stark, H., Goldan, P. D., Kuster, W. C., Bates, T. S., Coffman, D., Ravishankara, A. R., and Brown, S. S.: Observation of daytime N2O5in the marine boundary layer during New England Air Quality Study-Intercontinental Transport and Chemical Transformation 2004, Journal of Geophysical Research: Atmospheres, 111, n/a-n/a, 10.1029/2006jd007593, 2006.

Pathak, R. K., and W.S.Wu: Summertime PM2.5 ionic species in four major cities of China; nitrate formation in an ammonia-deficient atmosphere, Atmospheric Chemistry and Physics, 9, 1711-1722, 2009.

Pathak, R. K., Wang, T., and Wu, W. S.: Nighttime enhancement of PM2.5 nitrate in ammonia-poor atmospheric conditions in Beijing and Shanghai: Plausible contributions of heterogeneous

582 hydrolysis of N2O5 and HNO3 partitioning, Atmospheric Environment, 45, 1183-1191,
583 10.1016/j.atmosenv.2010.09.003, 2011.

584 Petetin, H., Sciare, J., Bressi, M., Gros, V., Rosso, A., Sanchez, O., Sarda-Estève, R., Petit, J.-E., and
585 Beekmann, M.: Assessing the ammonium nitrate formation regime in the Paris megacity and its
586 representation in the CHIMERE model, Atmospheric Chemistry and Physics, 16, 10419-10440,
587 10.5194/acp-16-10419-2016, 2016.

588 Pusede, S. E., Duffey, K. C., Shusterman, A. A., Saleh, A., Laughner, J. L., Wooldridge, P. J., Zhang, Q.,
589 Parworth, C. L., Kim, H., Capps, S. L., Valin, L. C., Cappa, C. D., Fried, A., Walega, J., Nowak, J.
590 B., Weinheimer, A. J., Hoff, R. M., Berkoff, T. A., Beyersdorf, A. J., Olson, J., Crawford, J. H., and
591 Cohen, R. C.: On the effectiveness of nitrogen oxide reductions as a control over ammonium nitrate
592 aerosol, Atmospheric Chemistry and Physics, 16, 2575-2596, 10.5194/acp-16-2575-2016, 2016.

593 Riemer, N.: Impact of the heterogeneous hydrolysis of N2O5on chemistry and nitrate aerosol formation
594 in the lower troposphere under photosmog conditions, Journal of Geophysical Research, 108,
595 10.1029/2002jd002436, 2003.

596 Rumsey, I. C., Cowen, K. A., Walker, J. T., Kelly, T. J., Hanft, E. A., Mishoe, K., Rogers, C., Proost, R.,
597 Beachley, G. M., Lear, G., Frelink, T., and Otjes, R. P.: An assessment of the performance of the
598 Monitor for AeRosols and GAses in ambient air (MARGA): a semi-continuous method for soluble
599 compounds, Atmospheric Chemistry and Physics, 14, 5639-5658, 10.5194/acp-14-5639-2014, 2014.

600 Seinfeld, J. H., and Pandis, S. N.: Atmospheric Chemistry and Physics: From Air Pollution to Climate
601 Change, John Wiley & Sons, New York, 2nd edition, 1232 pp., 13: 978-0-471-72018-8 2006.

602 Sharma, M., Kishore, S., Tripathi, S. N., and Behera, S. N.: Role of atmospheric ammonia in the
603 formation of inorganic secondary particulate matter: A study at Kanpur, India, Journal of
604 Atmospheric Chemistry, 58, 1-17, 10.1007/s10874-007-9074-x, 2007.

605 Shen, Y., Virkkula, A., Ding, A., Wang, J., Chi, X., Nie W., Qi, X., Huang, X., Liu Q., Zheng, L., Xu, Z.,
606 Petaja, T., Aalto, P.P., Fu, C. and Kulmala, M.: Aerosol optical properties at SORPES in Nanjing,
607 East China, Atmos. Chem. Phys., 18, 5265-5292, 2018.

608 Shi, Y., Chen, J., Hu, D., Wang, L., Yang, X., and Wang, X.: Airborne submicron particulate (PM1)
609 pollution in Shanghai, China: chemical variability, formation/dissociation of associated semi-
610 volatile components and the impacts on visibility, The Science of the total environment, 473-474,
611 199-206, 10.1016/j.scitotenv.2013.12.024, 2014.

612 Sun, Y. L., Zhang, Q., Schwab, J. J., Demerjian, K. L., Chen, W. N., Bae, M. S., Hung, H. M., Hogrefe,
613 O., Frank, B., Rattigan, O. V., and Lin, Y. C.: Characterization of the sources and processes of
614 organic and inorganic aerosols in New York city with a high-resolution time-of-flight aerosol mass
615 apectrometer, Atmospheric Chemistry and Physics, 11, 1581-1602, 10.5194/acp-11-1581-2011,
616 2011.

617 ten Brink, H., Otjes, R., Jongejan, P., and Slanina, S.: An instrument for semi-continuous monitoring of
618 the size-distribution of nitrate, ammonium, sulphate and chloride in aerosol, Atmospheric

Environment, 41, 2768-2779, 10.1016/j.atmosenv.2006.11.041, 2007.

Thornton, J. A., Braban, C. F., and Abbatt, J. P. D.: N2O5 hydrolysis on sub-micron organic aerosols: the effect of relative humidity, particle phase, and particle size, Phys Chem Chem Phys, 5, 4593-4603, 2003

van der A, R. J., Mijling, B., Ding, J., Koukouli, M. E., Liu, F., Li, Q., Mao, H., and Theys, N.: Cleaning up the air: effectiveness of air quality policy for SO2 and NOx emissions in China, Atmospheric Chemistry and Physics, 17, 1775-1789, 10.5194/acp-17-1775-2017, 2017.

Vayenas, D. V., Takahama, S., Davidson, C. I., and Pandis, S. N.: Simulation of the thermodynamics and removal processes in the sulfate-ammonia-nitric acid system during winter: Implications for PM2.5 control strategies, J Geophys Res-Atmos, 110, 2005.

Wang, D., Zhou, B., Fu, Q., Zhao, Q., Zhang, Q., Chen, J., Yang, X., Duan, Y., and Li, J.: Intense secondary aerosol formation due to strong atmospheric photochemical reactions in summer: observations at a rural site in eastern Yangtze River Delta of China, The Science of the total environment, 571, 1454-1466, 10.1016/j.scitotenv.2016.06.212, 2016a.

Wang, H.L., Qiao, L.P., Lou S.R., Zhou, M., Ding, A.J., Huang, H.Y., Chen, J.M., Wang, Q., Tao, S.K., Chen, C.H., Li L., and Huang C.: Chemical composition of PM2.5 and meterological impact among three years in urban Shanghai, China, Journal of Cleaner Proeuction, 112, 2, 1302-1311, 2016b.

Wang, H., Lu, K., Chen, X., Zhu, Q., Chen, Q., Guo, S., Jiang, M., Li, X., Shang, D., Tan, Z., Wu, Y., Wu, Z., Zou, Q., Zheng, Y., Zeng, L., Zhu, T., Hu, M., and Zhang, Y.: High N2O5 Concentrations Observed in Urban Beijing: Implications of a Large Nitrate Formation Pathway, Environmental Science & Technology Letters, 4, 416-420, 10.1021/acs.estlett.7b00341, 2017.

Wang, J., Ge, X., Chen, Y., Shen, Y., Zhang, Q., Sun, Y., Xu, J., Ge, S., Yu, H., and Chen, M.: Highly time-resolved urban aerosol characteristics during springtime in Yangtze River Delta, China: insights from soot particle aerosol mass spectrometry, Atmospheric Chemistry and Physics, 16, 9109-9127, 10.5194/acp-16-9109-2016, 2016c.

Wang, J., Zhao, B., Wang, S., Yang, F., Xing, J., Morawska, L., Ding, A., Kulmala, M., Kerminen, V.-M., Kujansuu, J., Wang, Z., Ding, D., Zhang, X., Wang, H., Tian, M., Petäjä, T., Jiang, J., Hao, J., Particulate matter pollution over China and the effects of control policies, Science of the Total Environment, 584, 426-447, 2017.

Wang, T., Nie, W., Gao, J., Xue, L. K., Gao, X. M., Wang, X. F., Qiu, J., Poon, C. N., Meinardi, S., Blake, D., Wang, S. L., Ding, A. J., Chai, F. H., Zhang, Q. Z., and Wang, W. X.: Air quality during the 2008 Beijing Olympics: secondary pollutants and regional impact, Atmospheric Chemistry and Physics, 10, 7603-7615, 2010.

Wang, X., and Zhang, Y.: Particulate Nitrate Formation in a Highly Polluted Urban Area: A Case Study by Single-Particle Mass Spectrometry in Shanghai Environ. Sci. Technol, 43, 3061-3066, 2009.

Wang, X., Ding, X., Fu, X., He, Q., Wang, S., Bernard, F., Zhao, X., and Wu, D.: Aerosol scattering coefficients and major chemical compositions of fine particles observed at a rural site in the central

Pearl River Delta, South China, Journal of Environmental Sciences, 24, 72-77, 10.1016/s1001-0742(11)60730-4, 2012.

Wang, X. F., Chen, J. M., Sun, J. F., Li, W. J., Yang, L. X., Wen, L., Wang, W. X., Wang, X. M., Collett, J. L., Shi, Y., Zhang, Q. Z., Hu, J. T., Yao, L., Zhu, Y. H., Sui, X., Sun, X. M., and Mellouki, A.: Severe haze episodes and seriously polluted fog water in Ji'nan, China, Sci Total Environ, 493, 133-137, 2014.

Wen, L., Chen, J., Yang, L., Wang, X., Caihong, X., Sui, X., Yao, L., Zhu, Y., Zhang, J., Zhu, T., and Wang, W.: Enhanced formation of fine particulate nitrate at a rural site on the North China Plain in summer: The important roles of ammonia and ozone, Atmospheric Environment, 101, 294-302, 10.1016/j.atmosenv.2014.11.037, 2015.

Wen, L., Xue, L., Wang, X., Xu, C., Chen, T., Yang, L., Wang, T., and Wang, W.: Summertime fine particulate nitrate pollution in the North China Plain: Increasing trends, formation mechanisms, and implications for control policy, Atmos. Chem. Phys. Discuss., https://doi.org/10.5194/acp-2018-89, in review, 2018.

Xie, Y., Ding, A., and Nie, W.: Enhanced sulfate formation by nitrogen dioxide: Implications from in situ observations at the SORPES station Journal Of Geophysical Research: Atmospheres, 120, 12,679-612,964, 10.1002/, 2015.

Xue., J., and Yuan., Z.: Insights into factors afferting nitrate in PM2.5 in a polluted high NOx environment through hourly observations and size distribution measurements Journal of Geophysical Research: Atmospheres, 119, 4888-4902, 10.1002/, 2013.

Yang, T., Sun, Y., Zhang, W., Wang, Z., Liu, X., Fu, P., and Wang, X.: Evolutionary processes and sources of high-nitrate haze episodes over Beijing, Spring, J Environ Sci (China), 54, 142-151, 10.1016/j.jes.2016.04.024, 2017.

Young, D. E., Kim, H., Parworth, C., Zhou, S., Zhang, X., Cappa, C. D., Seco, R., Kim, S., and Zhang, Q.: Influences of emission sources and meteorology on aerosol chemistry in a polluted urban environment: results from DISCOVER-AQ California, Atmospheric Chemistry and Physics, 16, 5427-5451, 10.5194/acp-16-5427-2016, 2016.

Zhang, Q., Canagaratna, M. R., Jayne, J. T., Worsnop, D. R., and Jimenez, J. L.: Time- and size-resolved chemical composition of submicron particles in Pittsburgh: Implications for aerosol sources and processes, J Geophys Res-Atmos, 110, 2005.

Zhang, Y., Tang, L., Yu, H., Wang, Z., Sun, Y., Qin, W., Chen, W., Chen, C., Ding, A., Wu, J., Ge, S., Chen, C., and Zhou, H.-c.: Chemical composition, sources and evolution processes of aerosol at an urban site in Yangtze River Delta, China during wintertime, Atmospheric Environment, 123, 339-349, 10.1016/j.atmosenv.2015.08.017, 2015a.

Zhang, Y. J., Tang, L. L., Wang, Z., Yu, H. X., Sun, Y. L., Liu, D., Qin, W., Canonaco, F., Prévôt, A. S. H., Zhang, H. L., and Zhou, H. C.: Insights into characteristics, sources, and evolution of submicron aerosols during harvest seasons in the Yangtze River delta region, China, Atmospheric Chemistry

and Physics, 15, 1331-1349, 10.5194/acp-15-1331-2015, 2015b.

Zhang, Y. W., Zhang, X. Y., Zhang, Y. M., Shen, X. J., Sun, J. Y., Ma, Q. L., Yu, X. M., Zhu, J. L., Zhang, L., and Che, H. C.: Significant concentration changes of chemical components of PM1 in the Yangtze River Delta area of China and the implications for the formation mechanism of heavy haze-fog pollution, The Science of the total environment, 538, 7-15, 10.1016/j.scitotenv.2015.06.104, 2015c.

Zhang, Y., Ding, A., Mao, H., Nie, W., Zhou, D., Liu, L., Huang, X., and Fu, C.: Impact of synoptic weather patterns and inter-decadal climate variability on air quality in the North China Plain during 1980-2013, Atmos. Environ., 124, 119-128, 2016.

Zou, J., Liu, Z., Hu, B., Huang, X., Wen, T., Ji, D., Liu, J., Yang, Y., Yao, Q., and Wang, Y.: Aerosol chemical compositions in the North China Plain and the impact on the visibility in Beijing and Tianjin, Atmospheric Research, 201, 235-246, 10.1016/j.atmosres.2017.09.014, 2018.

Atmos. Chem. Phys. Discuss., https://doi.org/10.5194/acp-2018-608
Manuscript under review for journal Atmos. Chem. Phys.
Discussion started: 2 July 2018

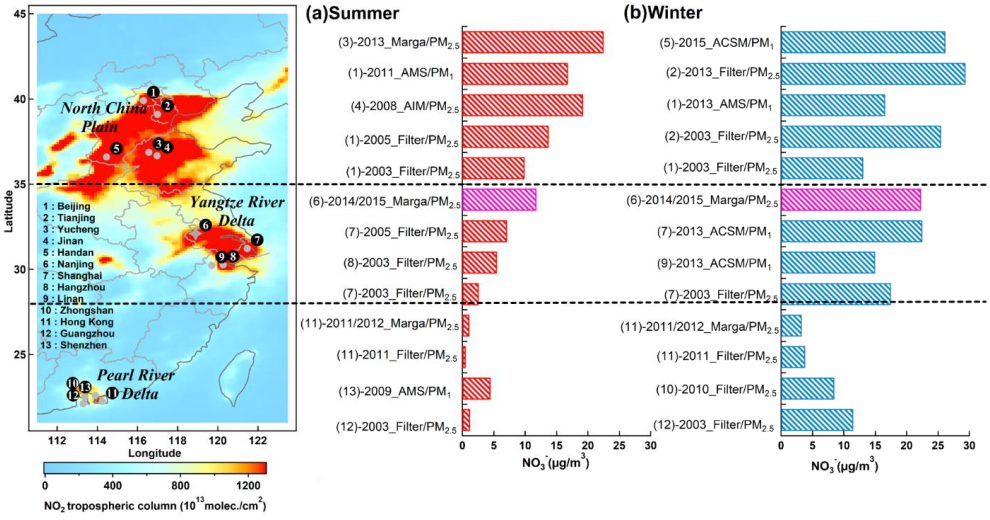

Figure 1 Average mass concentrations of particulate nitrate at different sampling sites in **(a)** summer and **(b)** winter. The left panel shows the map color-coded by 2-years (2014-2015) averaged tropospheric NO_2 from OMI satellite (http://www.temis.nl/airpollution/no2.html). The pink bars are for this study.

Atmos. Chem. Phys. Discuss., https://doi.org/10.5194/acp-2018-608
Manuscript under review for journal Atmos. Chem. Phys.
Discussion started: 2 July 2018

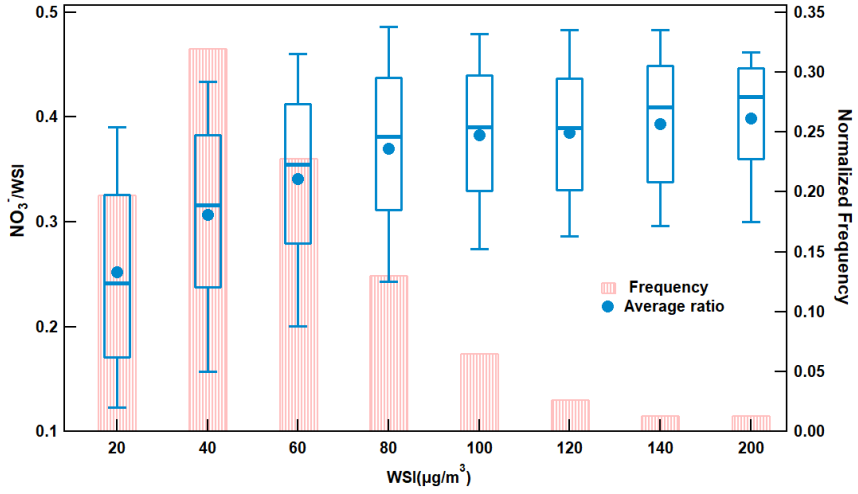

Figure 2 Average proportion of nitrate and normalized frequency of occurrence at different mass concentration bins of water soluble ions at SORPES. For the ratio, box boundaries represent the interquartile range, bars represent 5%-95% percentile range, and horizontal lines represent the median value.

Atmos. Chem. Phys. Discuss., https://doi.org/10.5194/acp-2018-608
Manuscript under review for journal Atmos. Chem. Phys.
Discussion started: 2 July 2018

Atmospheric Chemistry and Physics Discussions

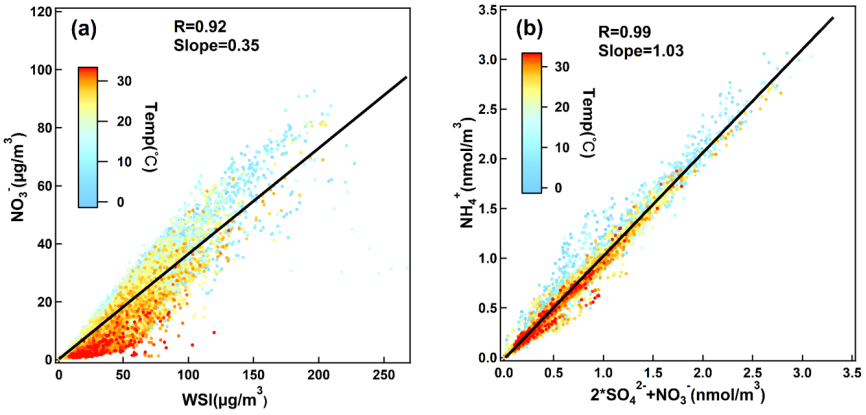

Figure 3 Scatter plots of **(a)** nitrate vs. total WSI color coded by air temperature, **(b)** molar concentrations of ammonium with nitrate molar concentrations plus two times of sulfate molar concentrations.

Atmos. Chem. Phys. Discuss., https://doi.org/10.5194/acp-2018-608
Manuscript under review for journal Atmos. Chem. Phys.
Discussion started: 2 July 2018

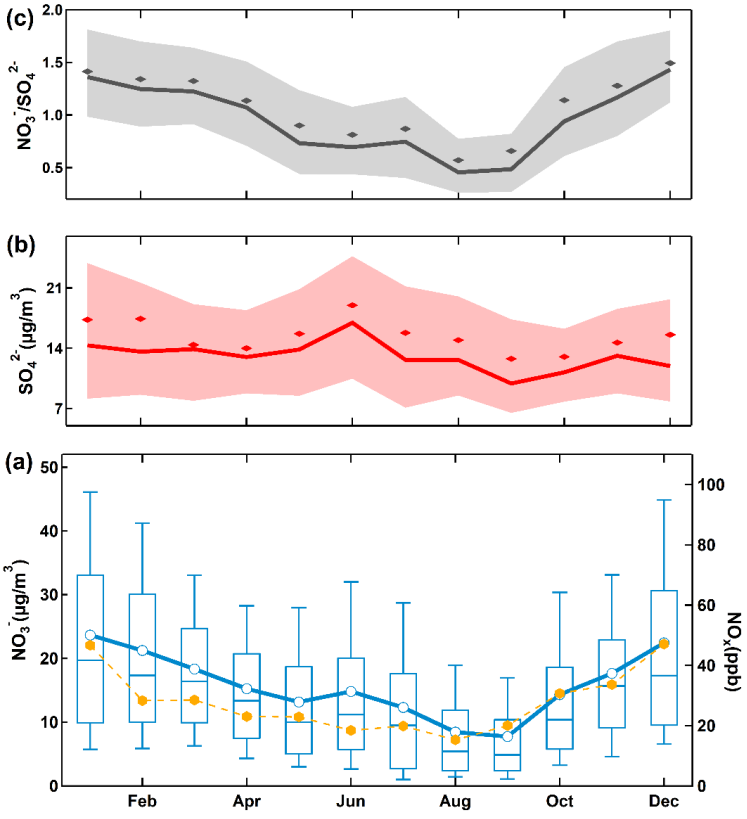

Figure 4 Monthly averaged nitrate (blue), sulfate (red), NO_x (orange) mass concentrations and nitrate to sulfate ratio (grey) measured at SORPES station during March 2014 to February 2016. For nitrate to sulfate ratio (a) and sulfate (b), bold solid lines are the median values, shade areas represent percentiles of 75% and 25%, and diamonds represent the mean values. For nitrate (c), box boundaries represent the interquartile range, bars represent 5%-95% percentile range, horizontal lines represent the median value, and crosses represent mean values.

Atmos. Chem. Phys. Discuss., https://doi.org/10.5194/acp-2018-608
Manuscript under review for journal Atmos. Chem. Phys.
Discussion started: 2 July 2018

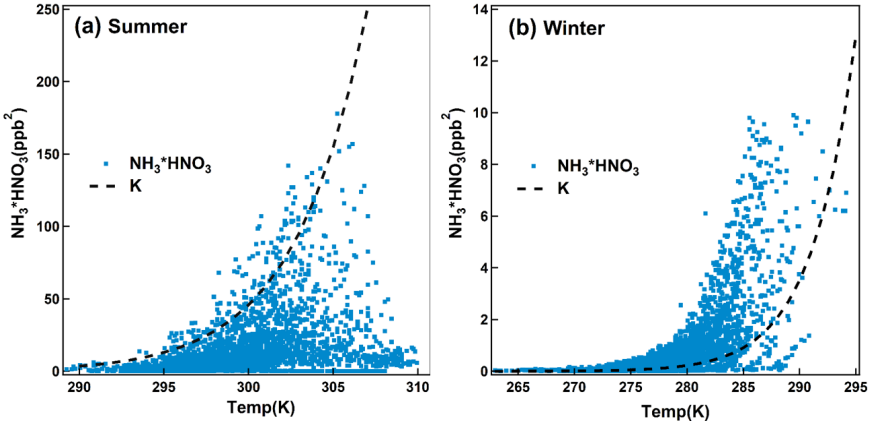

Figure 5 Scatter plot of product of [NH_3(g)]*[HNO_3(g)] with temperature together with the K parameter calculated by temperature for **(a)** summer and **(b)** winter.

Atmos. Chem. Phys. Discuss., https://doi.org/10.5194/acp-2018-608
Manuscript under review for journal Atmos. Chem. Phys.
Discussion started: 2 July 2018

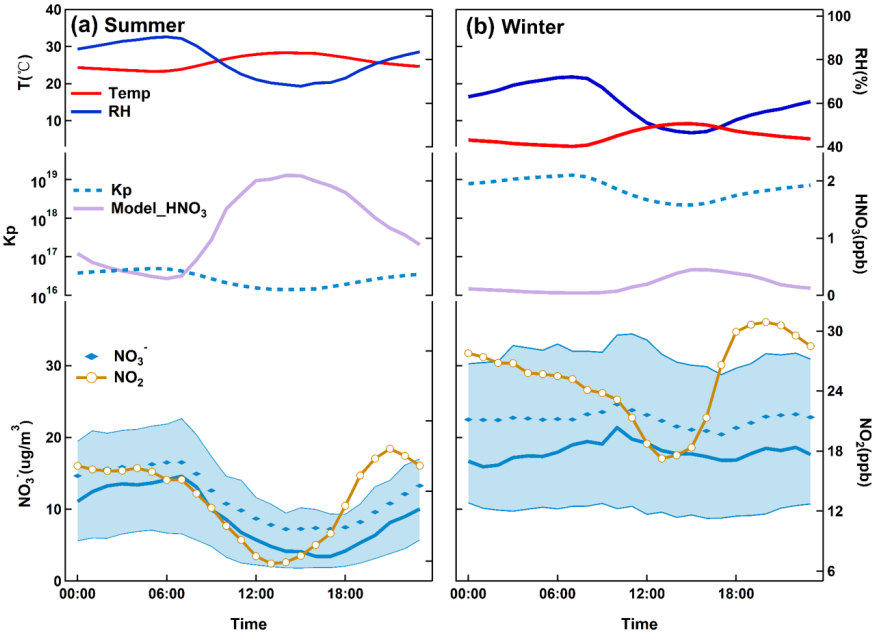

Figure 6 Diurnal variation of particulate nitrate in **(a)** summer and **(b)** winter. For nitrate, bold solid lines are the median values, shaded areas represent percentiles of 75% and 25% and diamonds represent mean values. Diurnal averages of NO_2 and modeled nitric acid mass concentrations are also provided with temperature and RH.

Atmos. Chem. Phys. Discuss., https://doi.org/10.5194/acp-2018-608
Manuscript under review for journal Atmos. Chem. Phys.
Discussion started: 2 July 2018

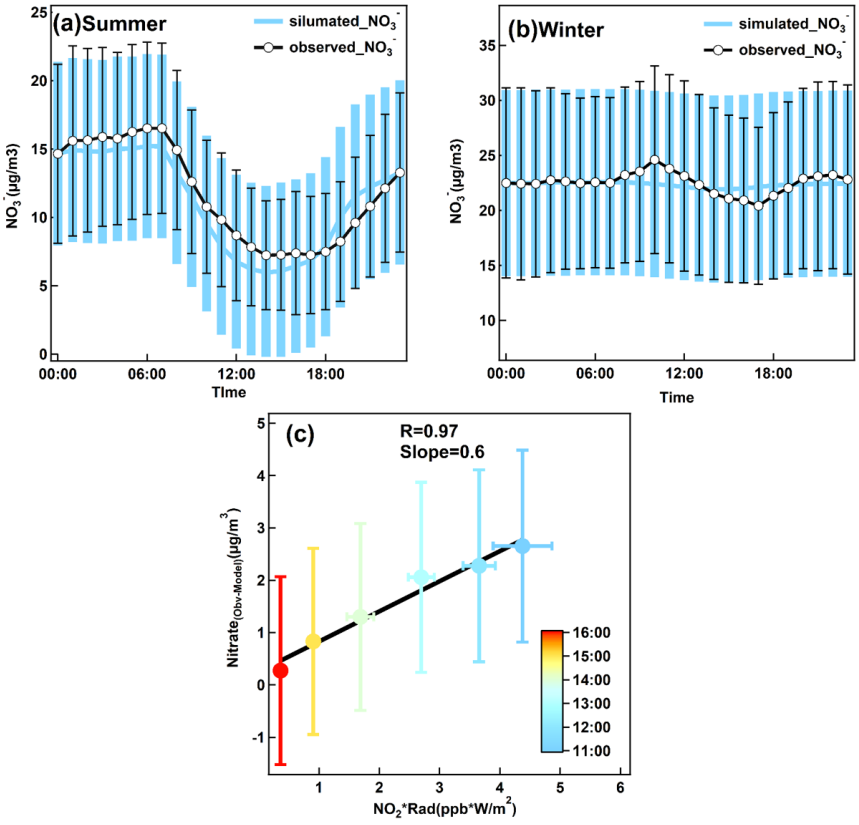

Figure 7 Modeled nitrate diurnal variations in **(a)** summer and **(b)** winter, together with the observed nitrate concentrations. Error bars provided are the standard deviation of the mean at each hourly interval. **(c)** Scatter plot of the difference between model and observed nitrate average mass concentrations with the product of NO_2 and radiation color coded by the hour of day for the samples.

Atmos. Chem. Phys. Discuss., https://doi.org/10.5194/acp-2018-608
Manuscript under review for journal Atmos. Chem. Phys.
Discussion started: 2 July 2018

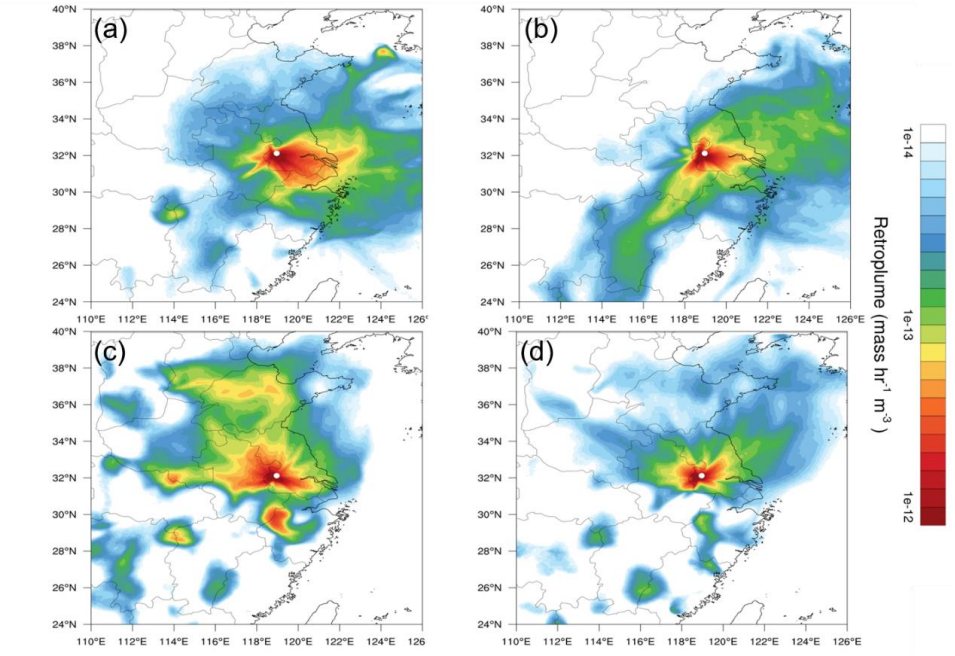

Figure 8 The averaged retroplumes (i.e., 100 m footprint) of the selected events: **(a)** Top 25% nitrate concentrations in summer, **(b)** Bottom 25% nitrate concentrations in summer, **(c)** Top 25% nitrate concentrations in winter, and **(d)** Bottom 25% nitrate concentrations in winter.

Atmos. Chem. Phys. Discuss., https://doi.org/10.5194/acp-2018-608
Manuscript under review for journal Atmos. Chem. Phys.
Discussion started: 2 July 2018

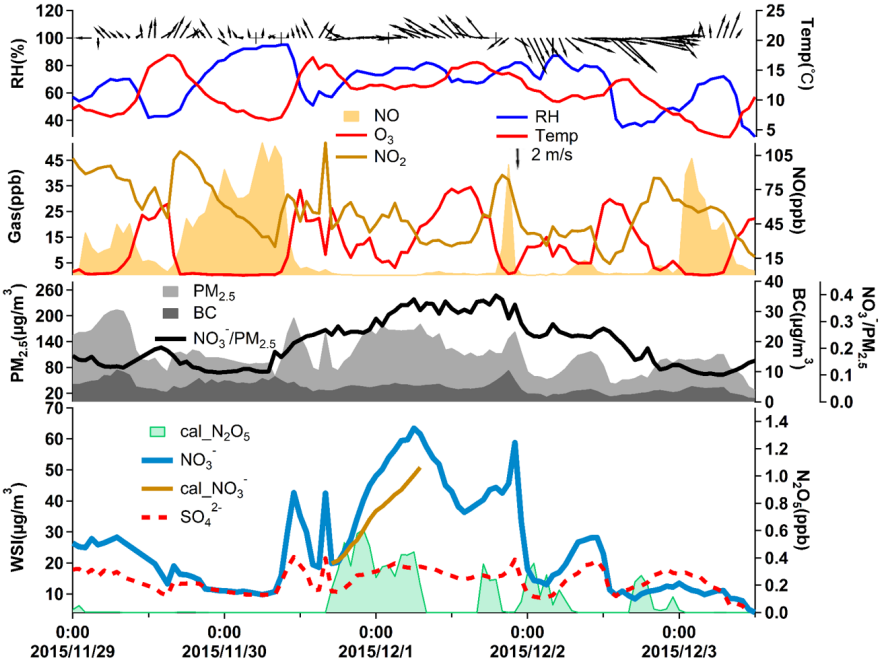

Figure 9 Time series of meteorological data and the concentrations of trace gases related to nitrate formation during 29 November to 3 December, 2015. Cal_NO_3^- represents the nitrate concentrations calculated from the hydrolysis of N_2O_5.

Atmos. Chem. Phys. Discuss., https://doi.org/10.5194/acp-2018-608
Manuscript under review for journal Atmos. Chem. Phys.
Discussion started: 2 July 2018

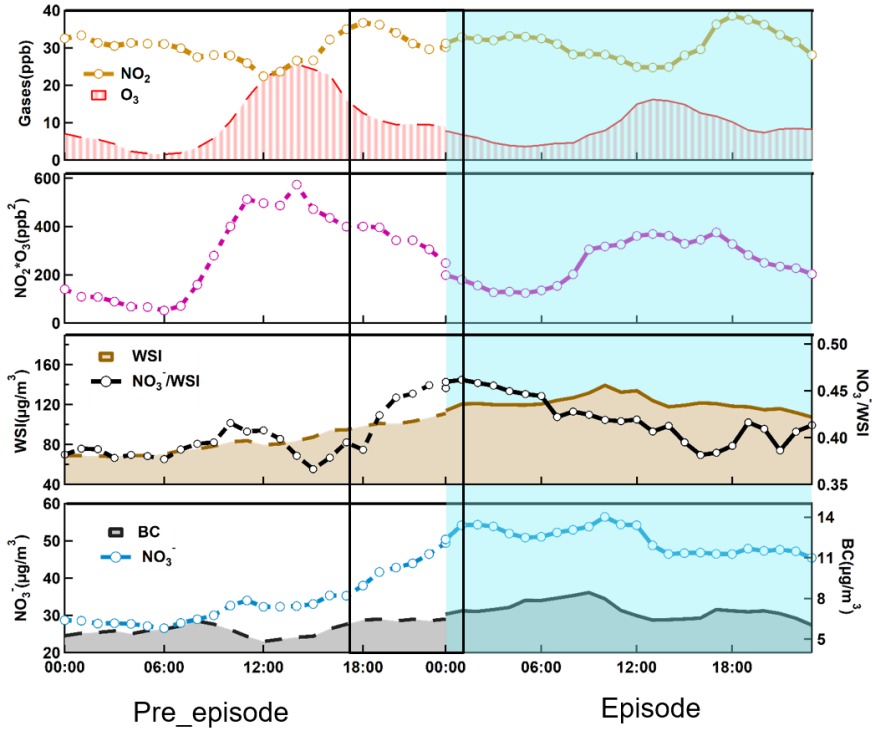

Figure 10 Diurnal variations of particulate nitrate, black carbon, the total water soluble ions, nitrate to WSI ratio, product of NO_2 and O_3, NO_2, and O_3 averaged for nitrate episode days with exceedances of one mean plus two standard deviations. The left side shows the pre-episode days and the right side shows the episode days during the winter of entire two years period. The solid line box corresponds to the rapid growth of nitrate at night.

Atmos. Chem. Phys. Discuss., https://doi.org/10.5194/acp-2018-608
Manuscript under review for journal Atmos. Chem. Phys.
Discussion started: 2 July 2018

Atmospheric Chemistry and Physics Discussions

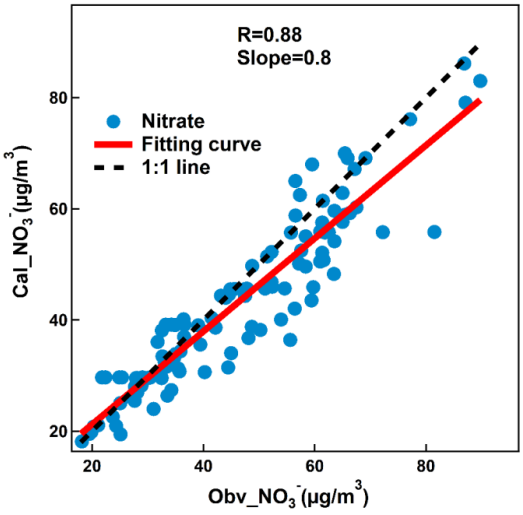

Figure 11 Scatter plot of calculated nitrate concentrations and observed nitrate concentrations from 17:00 to 23:00 of each episode.

Atmos. Chem. Phys. Discuss., https://doi.org/10.5194/acp-2018-608
Manuscript under review for journal Atmos. Chem. Phys.
Discussion started: 2 July 2018

Atmospheric Chemistry and Physics Discussions

Table 1 major gas phase and heterogeneous reactions involved NO_3 and N_2O_5

Reaction	Rate constant
$NO_2+O_3 \rightarrow NO_3+O_2$	k_1
$NO_3+NO_2 \leftrightarrow N_2O_5$	k_{eq}
$NO_3+NO \leftrightarrow NO_2+NO_2$	k_3
$NO_3 \rightarrow NO+O_2$	j_4
$NO_3 \rightarrow NO+O_2$	j_5
$NO_3 \xrightarrow{voc}$ products	$k_6=\sum(k_{voci}\cdot[voc]_i)$
$NO_3 \xrightarrow{Heterogeneous}$ products	$k_7=0.25\cdot i\cdot C_{NO_3}\cdot\gamma_{NO_3}\cdot S_{aerosol}$
$N_2O_5 \xrightarrow{Heterogeneous}$ products	$k_8=0.25\cdot C_{N_2O_5}\cdot\gamma_{N_2O_5}\cdot S_{aerosol}$
$N_2O_5 \xrightarrow{Homogeneous} 2HNO_3$	$k_9=k_I\cdot[H_2O]+k_{II}\cdot[H_2O]^2$